

Fabrication of microfluidic structures in quartz via micro machining technologies

Ying-Chieh Lin¹ · Chung-Ching Lee¹ · Heng-Sheng Lin¹ · Zheng-Han Hong² · Fu-Chuan Hsu² · Tsung-Pin Hung² · Yu-Ting Lyu²

Received: 9 June 2015 / Accepted: 29 October 2015 / Published online: 30 December 2015
© Springer-Verlag Berlin Heidelberg 2015

Abstract Microfluidic channels have been created for quartz material using micromechanical manufacturing technologies such as micro laser machining, micro ultrasonic machining, and ultra-precision machining. Ultra-precision machining has been used to manufacture cross-junction channels 14 μm wide and 28 μm deep with a three-dimensional triangle cross-section. Micro laser machining has been used to manufacture U-shaped and \sqsubset -shaped microfluidic channels. Deep holes and microfluidic channels with a high slenderness ratio (width/depth) can be obtained by using micro ultrasonic machining technology. These three machining techniques are compared with respect to surface profiles and machining quality.

1 Introduction

The rapid development of microfluidic channel has created a new platform for fabricating controllable microspheres via droplet formation (Leng et al. 2010; Anderson et al. 2009; Chu et al. 2007; Utada et al. 2005). Microfluidic channel control technology for producing microspheres have advantages such as good size controllability (Hisamoto et al. 2001), high reaction efficiency (Dittrich and Manz 2006), short process time (Brivio et al. 2006),

easy operation (Mitchell et al. 2001), and batch production. To produce a variety of chemical and biological reactions in a microfluidic device, the mobility of the merge, mix, and split for the chemical reactions can be controlled (Bokenkamp et al. 1998; Stroock et al. 2002; Hettiarachchi et al. 2007).

To create a micro-channel device, the selections of materials and machining method are critical. Materials commonly used of microfluidic channels include single-crystal silicon chips, glass, metals, and polymers. Single-crystal silicon has good thermal stability and chemical inertness, allowing high-precision three-dimensional (3D) structures to be produced. PMMA and poly-dimethylsiloxane (PDMS) are easily processed and low cost, making them very suitable for mass production. However, these materials have low melting points and poor material strength. Glass materials are commonly used as biochips for biological applications due to their biocompatibility and ease of reuse. Therefore, glass-based chips are commonly used in research and development units. However, the brittleness of glass make it difficult to process and control with precision. Therefore, the development of high-quality and high-precision micro-manufacturing methods for glass-based materials is necessary (Zhang et al. 2004, 2006; Yang et al. 2001). Various techniques have been applied to control microfluidic channels, including mechanical machining methods such as micro-milling (Nakano et al. 2007), micro ultrasonic machining, and micro electrical discharge machining (EDM), lithographic and electrolytic etching (Menezes et al. 2010; Borghi et al. 2008), as well as energy beam technology such as ultra-short-pulse laser machining (Gattass and Mazur 2008).

Although lithographic and electrolytic etching is commonly used for fabricating the two-dimensional (2D) micro-channels, the fabrication of 3D microfluidic

✉ Zheng-Han Hong
zheng@mail.mirdc.org.tw

¹ Department of Mold and Die Engineering,
National Kaohsiung University of Applied Sciences,
Kaohsiung 807, Taiwan

² Mold and Precision Machining Technology Section,
Micro/Meso Mechanical Manufacturing R&D Department,
Metal Industries Research and Development Centre
(MIRDC), Kaohsiung, Taiwan

structures requires stacking and bonding, leading to increased complexity and cost (Liu et al. 2012). Femtosecond laser technology has thus been used by many research groups for fabricating 3D microfluidic structures (Zheng and Lee 2005; Bhuyan et al. 2010; Queste et al. 2010; Liu et al. 2012).

Zheng and Lee (2005) used a CO₂ laser along the movement path of the beam to machining glass material removal. The formed groove was crack-free with a smooth bottom surface. Bhuyan et al. (2010) used a femtosecond laser to create the smallest tapered micro-channel in glass. The experimental results showed that the obtained microfluidic channels had a 2- μm diameter and aspect ratios of up to 40. Queste et al. (2010) manufactured microfluidic glass chips by using deep plasma etching, femtosecond laser ablation, and anodic bonding. The results showed that the obtained laser- and etching-cut microfluidic channels were 100 μm wide and 140 μm high, with a profile angle of 80°–85°. Liu et al. (2012) used a nanosecond laser to fabricate 3D microfluidic glass channels. Six micro-channels are fabricated 210 μm beneath the porous glass surface at pulse energies of 60, 120, 180, 160, 170, and 180 μJ , respectively, and three more micro-channels are fabricated 420 μm beneath the glass surface at pulse energies of 120, 160, and 180 μJ , respectively.

The fabrication of 3D microfluidic glass channels using laser processing is thus of interest. However, the roughness of the channel surface and machining accuracy are poor with laser machining. This study compares the performance of micro ultrasonic machining, ultra-short-pulse laser machining, and ultra-precision machining in fabricating 3D microfluidic channels in quartz.

2 Experimental methods

2.1 Materials and micro-manufacturing methods

Material properties are the first consideration for 3D microfluidic channels. The chosen material must have good chemical properties, such as biocompatibility and chemical stability. In addition, the quality and precision of micro-manufacturing methods depend on the material. Quartz was selected as the substrate material in the present study due to its low coefficient of thermal expansion, good wear resistance and biocompatibility, and high light penetration resistance. The brittleness of quartz makes it difficult to process and precisely control, making it a good test material.

Micro ultrasonic machining, ultra-short-pulse laser machining, and ultra-precision machining were used to fabricate 3D microfluidic glass structures.

2.2 Picosecond laser machining equipment and methods

Figure 1a shows the picosecond laser system (PL10100, Ekspla Co. Ltd.) used in the experiments. Its technical specifications are listed in Table 1. The laser parameters set for glass ablation were a 1064-nm wavelength, a pulse duration of 10 ps, a repetition rate of 50–100 kHz, a minimum focusing spot diameter 15 μm , and the circular polarization state, converted from the linear polarization state using a quarter-wave plate (QWP). The maximum incident pulse energy was chosen to be 0.2 mJ. The average output power was tuned from 0 to 10 W with adjustable power attenuation. A precision moving stage was mounted along

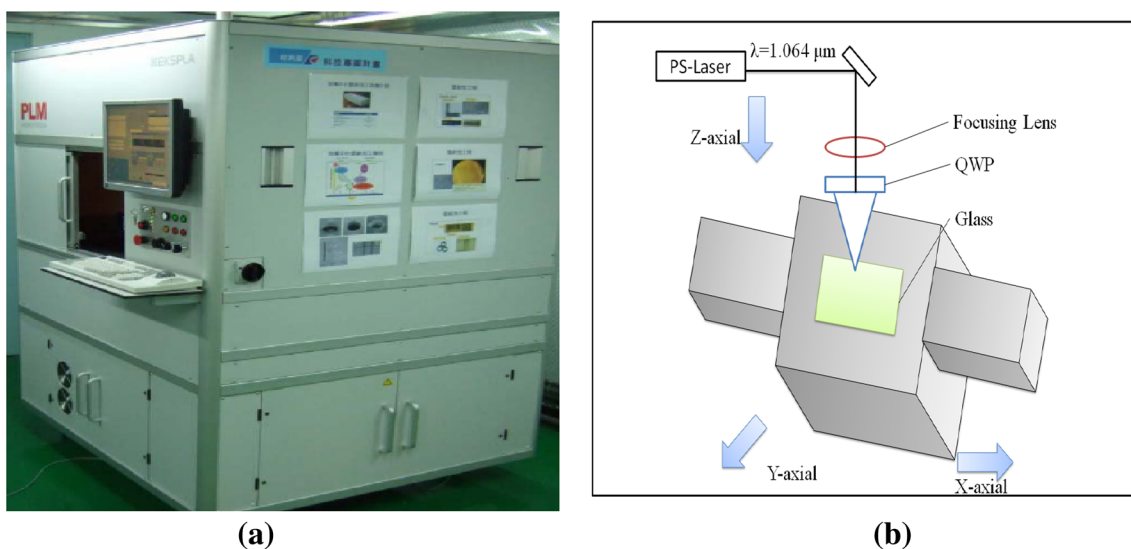


Fig. 1 **a** Ultra-short-pulse laser machining system and **b** schematic diagram of laser workstation for micro channel manufacturing

Table 1 Specifications of picosecond laser machining equipment

Item	Value
Wavelength	1064 nm
Average output power	>10 W
Maximum incident pulse energy	200 μ J @ 50 kHz
Repetition rate	50–100 kHz
Pulse duration	<10 ps
XYZ stage range	200 \times 200 \times 100 mm
Position accuracy	\pm 1 μ m

the 2-axis XY table translation on the horizontal plane with a maximum travel distance of 200 mm for each axis. The vertical moving stage had a maximum travel distance of 100 mm with 1- μ m position precision, as shown in Fig. 1b. To increase the machining accuracy, a charge-coupled device (CCD) camera connected to a computer was used to image the fabricated structure in real time.

In this study, a picosecond laser was used for manufacturing the desired geometry of microfluidic channels in quartz. The use of an ultrafast laser with a high repetition rate for processing quartz is favorable for surface cold-ablation quality and processing efficiency. Microfluidic channels with U- and \perp -shape geometries were fabricated.

2.3 Ultra-precision machining equipment and methods

An ultra-precision machining system, shown Fig. 2a, effectively manufactures structures with high geometrical accuracy and super smooth surfaces using a single-point diamond. It has been adopted to manufacture optical components for light guide plates, column mirror plate gratings, and retro-reflective plates. Such applications require extremely high geometrical accuracy for

Table 2 Specifications of ultra-precision machining equipment

Item	Value
Maximum machining size	300 \times 300 mm ²
Microstructure dimensions	Pitch 0.2–300 μ m Depth 0.1–120 μ m
Dimensional accuracy	\leq \pm 0.5 μ m
Surface roughness (R_a)	\leq 20 nm

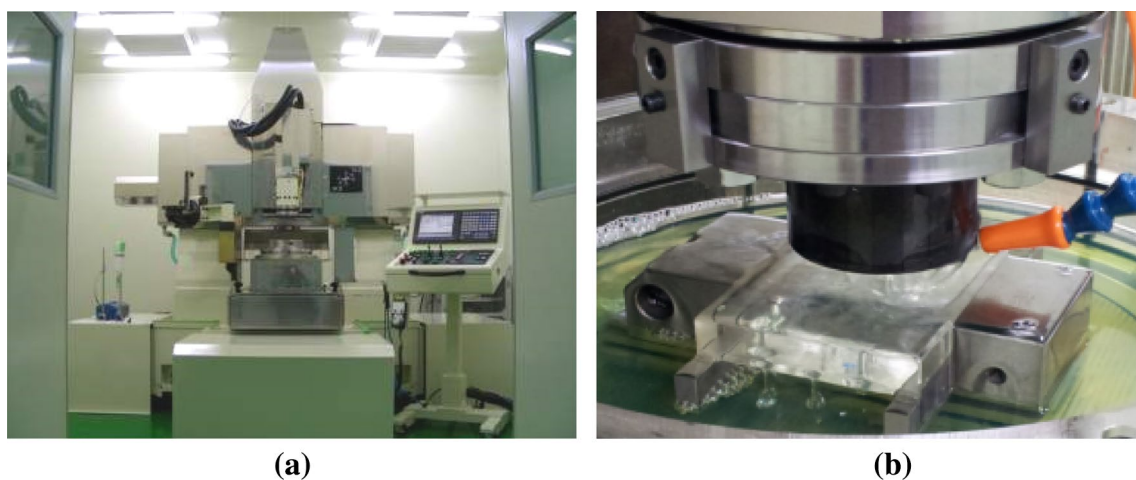
the machining of mirror surface microstructures (V- and R-grooves) and the micro-prism array structures, and super smooth surfaces.

The machinery developed for such applications typically requires only one actuator drive system for the linear axis of motion, which is implemented by a super-precision linear motor. By synchronizing the 1-nm resolution feed X, Y, and Z axes and the work rotation C axis, versatile machining is possible. The specifications of the ultra-precision machining system are listed in Table 2. Figure 2b shows a close-up photograph of the ultra-precision machining system.

2.4 Five-axis machine for ultrasonic-vibration-assisted milling and drilling

A five-axis machine combined with an ultrasonic-vibration-assisted machining chuck effectively manufactures structures in high-brittleness materials such as quartz and ceramics by using ultrasonic-vibration-assisted milling and drilling, as shown in Fig. 3a.

The rotational ultrasonic-vibration-assisted machining chuck was designed by the Metal Industries Research and Development Centre (MIRDC) (see Fig. 3b). The chuck total length and maximum diameter are 225 and

**Fig. 2** **a** Ultra-precision machining system and **b** close-up view

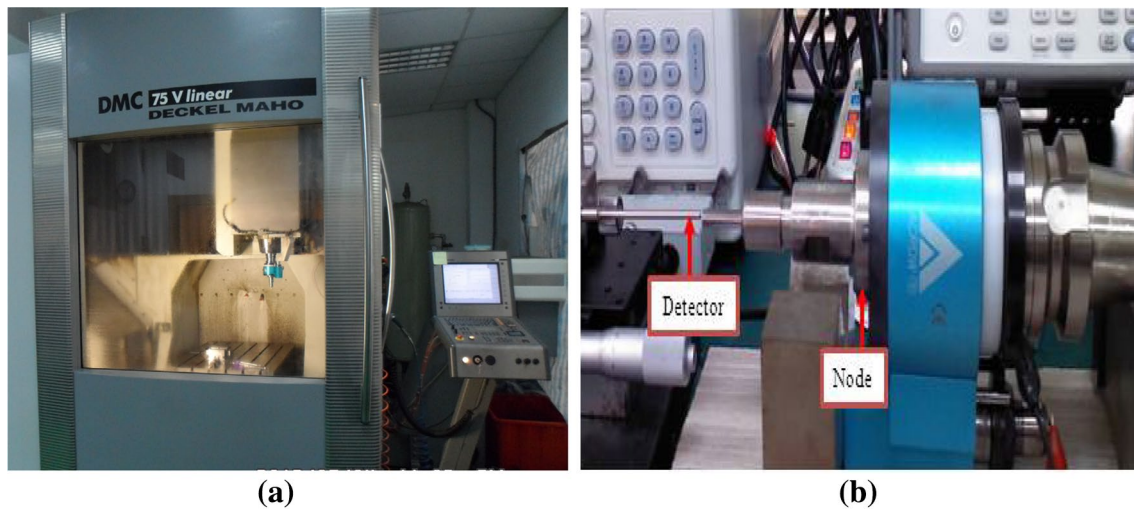


Fig. 3 **a** Five-axis milling machine, **b** ultrasonic-vibration-assisted machining chuck

128 mm, respectively. The transducer has a maximum amplitude in the axial direction at a resonance frequency of 21.9 kHz. In addition, simple harmonic motion is induced at a frequency of 19.8 kHz. The generator scans the frequency automatically before machining in the range of 18–22 kHz. Detailed specifications of the ultrasonic chuck and generator are shown in Table 3. The specifications of the five-axis milling machine are listed in Table 4. The five-axis dynamic milling and drilling, high speed, high efficiency, and low residual stress allow free-form surfaces to be created with good machining quality.

Table 3 Specifications of ultrasonic chuck

Item	Value
Length	225 mm
Maximum diameter	128 mm
Frequency	20 ± 2 kHz
Amplitude	3–10 μm
Maximum speed	8000 rpm
Runout	<5 μm
Working voltage	100–220 V

Table 4 Specifications of five-axis milling machine

Item	Value
Maximum machining size	750 × 600 × 500 mm
Minimum size of micro-holes	Φ 0.05 mm (aspect ratio ≥ 10)
Dimensional accuracy	$\leq \pm 0.5$ μm
Surface roughness (R_a)	≤ 20 nm

3 Results and discussion

3.1 Picosecond laser machining fabrication of microfluidic channels

Figure 4 shows the short-focusing lens and laser processing experiment setup. Through the horizontal displacement of the platform and a zoom displacement mechanism, a U-shaped cross-section micro-channel can be manufactured.

During the laser machining process, the machining speed was controlled at 20 mm/s, the output power was 5–10 W, and the pulse frequency was set to 50–100 kHz for process stability. In addition, third machining step from 1, 3, to 5 are considered for the different focal length.

A V-shaped deep groove with a width of 20 μm and a deep of 400 μm was obtained at an output power of 5 W, a pulse frequency of 100 kHz, a machining speed of 20 mm/s, and a focal length of 160 mm, as shown in Fig. 5. However, this geometry of substrate is bed to do microfluidic channel by 1st process due to strongest intensity on the beam waist and multi-photons material interaction for the Gaussian distribution of laser energy.

The channel length, channel arrangement, chambers length and direction of entrances and exits affect the single-phase low Reynolds number flow through the V-shaped grooves, Cross-section of a half circular microchannel (U-shaped microchannel) and Cross-section of a rectangle microchannel (\sqcup -shaped microchannel). To further evaluate the effects of the laser power, machining path, and processing order, U- and \sqcup -shaped microfluidic channels were produced by spatially accumulating V-shaped grooves. The width and depth of the V-shaped groove were 6 and 5 μm ,

Fig. 4 Experimental set-up of short-focusing lens adaptor for laser processing of micro-channel

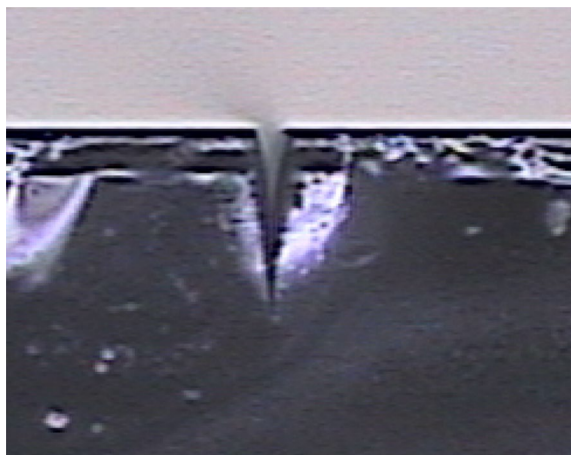
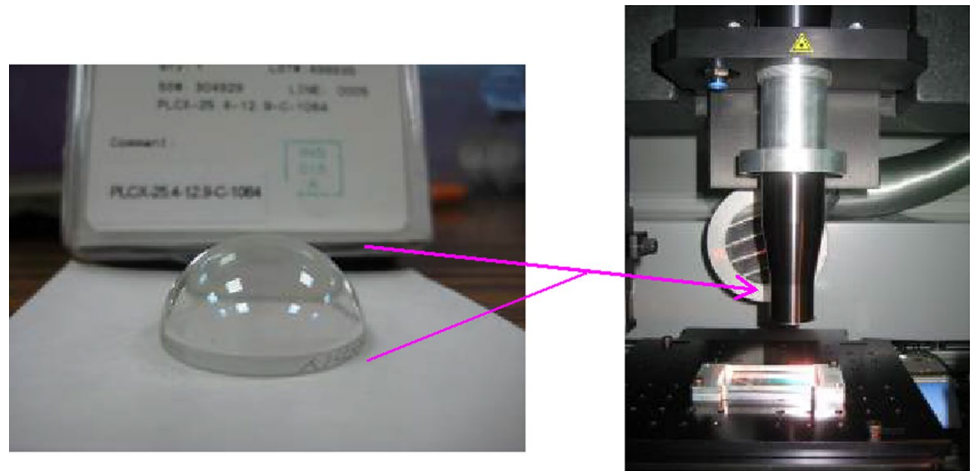


Fig. 5 Optical micrograph of cross section of V-shaped deep groove respectively, at an output power of 10 W, a pulse frequency of 75 kHz, and a focal length of 12 mm. Figure 6a shows an optical micrograph of the cross section of the 3D U-shaped

micro-channel. For investigating the cross sections of the 3D U-shaped micro-channel, the horizontal and zoom displacements were $5 \mu\text{m}/\text{step} \times 3$ steps and $3 \mu\text{m}/\text{step} \times 4$ steps, respectively. The machining path was from left to right. The cross section of the U-shaped channel was more rounded. From the top-view scanning electron microscopy (SEM) image of the cross section shown in Fig. 6b, the width was $21 \mu\text{m}$ and the depth was $23.8 \mu\text{m}$. There was an obvious crack at the inlet end due to edge effects, but the internal structure had good uniformity. Microcracks of less than $3 \mu\text{m}$ are acceptable for micro flow channels.

Figure 7a shows an optical micrograph of the cross section of the 3D U-shaped micro-channel. The horizontal and zoom displacements were $5 \mu\text{m}/\text{step} \times 3$ steps and $3 \mu\text{m}/\text{step} \times 4$ steps, respectively. The machining path was from inside to outside. From the top-view SEM image in Fig. 7b, the width was $19.5 \mu\text{m}$ and the depth was $18.8 \mu\text{m}$. There are some obvious cracks at the inlet end due to edge effects; however, the microcracks of less than $3 \mu\text{m}$ with

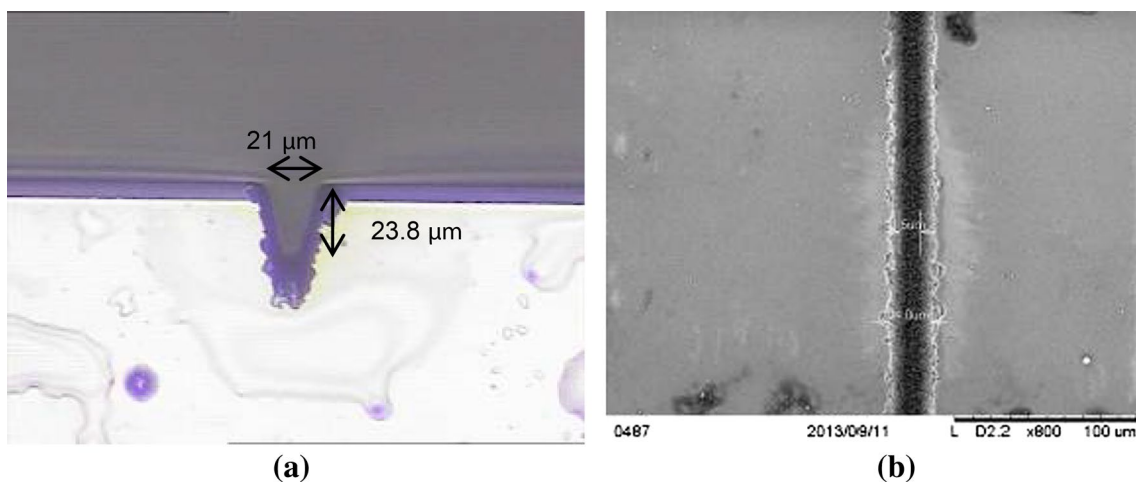


Fig. 6 a Optical micrograph of cross section of U-shaped microfluidic channel. b Top-view SEM image of microfluidic channel

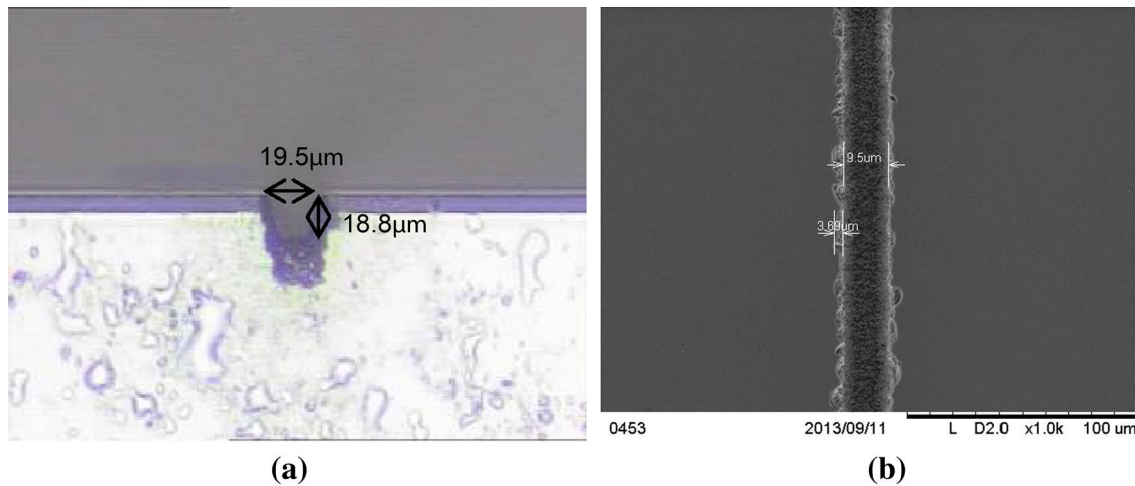


Fig. 7 **a** Optical micrograph of cross section of U-shaped microfluidic channel. **b** Top-view SEM image of microfluidic channel

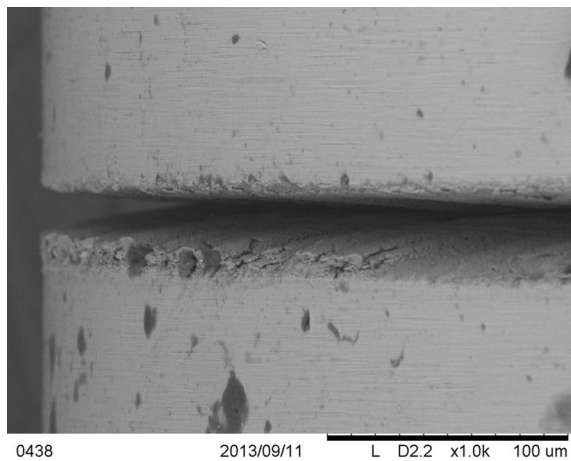


Fig. 8 SEM image of inner wall of microfluidic channel

good uniformity for the internal structure meet the specification requirements for micro flow channels. The experimental result is almost similar to the case of laser-induced plasma-assisted ablation using a 532-nm laser introduced

elsewhere (Zhang et al. 1998; Zhang and Midorikawa 1999).

A top-view SEM image of the morphology of the inner wall is shown in Fig. 8. The inner wall of the microfluidic channel has a relatively high surface roughness and a lot of slag.

3.2 Ultra-precision machining and micro ultrasonic machining fabrication of multi-functional microfluidic channels

Top-view optical micrographs of 3D channels in quartz fabricated using ultra-precision machining and micro ultrasonic machining are shown in Fig. 9. The V-shaped diamond cutting tools had an included angle of 90° and a clearance angle of 7° – 8° . A cross-junction channel with a width of $28\ \mu\text{m}$ and a depth of $14\ \mu\text{m}$ was obtained. The triangular cross section of the micro-channels (Fig. 10a) was obtained at a cutting depth of $1\ \mu\text{m}$, a cutting speed of $30\ \text{mm/min}$, and a temperature of $23 \pm 0.1\ ^\circ\text{C}$. The microfluidic channel surface was very smooth, without

Fig. 9 Optical micrograph of microfluidic channel fabricated using micro ultrasonic and ultra-precision machining

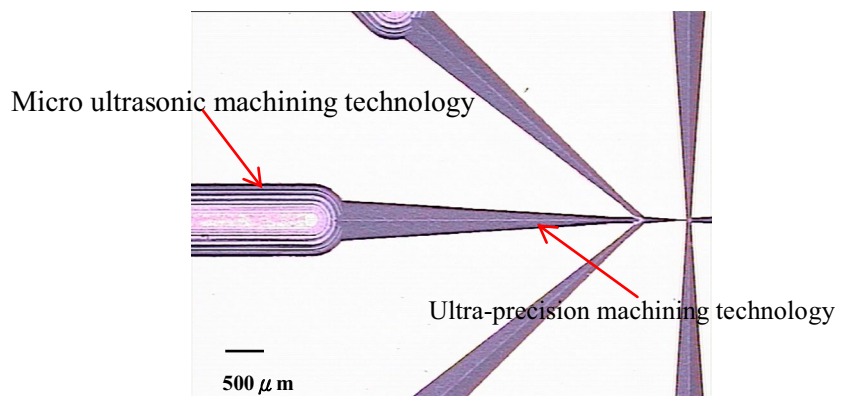
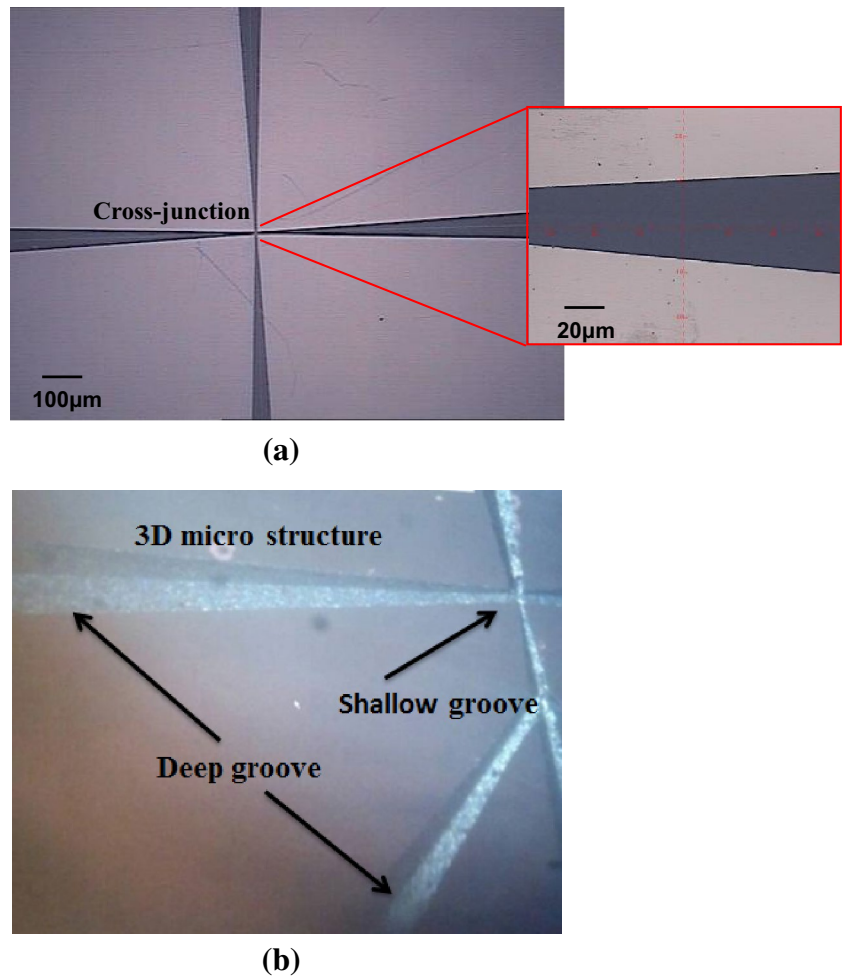


Fig. 10 **a** Optical micrograph of cross junction microfluidic channel. **b** Top-view optical micrograph of 3D microfluidic channel in quartz



chipping and cracks. The micro-channel surface roughness (R_a) was less than $0.27\ \mu\text{m}$ and good processing quality was obtained using ultra-precision machining. A 3D micro-structure with much smoother sidewalls was obtained using ultra-precision machining, with a depth of $14\text{--}100\ \mu\text{m}$, as shown in Fig. 10b.

To make a deep hole and fabricate a microfluidic channel with a high slenderness ratio (width/depth) in quartz, micro ultrasonic machining technology can be used. A diamond tool vibrating at a high frequency hits the surface of the workpiece in an abrasive slurry to force abrasive grains. High-slenderness-ratio microfluidic channels are machined into the quartz plate in the milling process. The machining parameters were: a rotational speed of 6000 rpm, a feed rate of 40 mm/min, and a temperature of $25 \pm 1\ ^\circ\text{C}$. A top-view optical micrograph of the microfluidic channels is shown in Fig. 11. The width and depth of the microfluidic channels are 1 mm and $350\ \mu\text{m}$, respectively. Many chips can be observed and the machined bottom surface is rough. The sidewalls have a much smoother surface than that of the bottom of the channel.

Deep holes were machined into the quartz plate in the drilling process. The 25-mm-thick plate of quartz was machined with ball end mills made of diamond. The machining parameters were: a rotational speed of 6000 rpm, a feed rate of 8 mm/min, and a temperature of $25 \pm 1\ ^\circ\text{C}$. A top-view optical micrograph of a 1-mm-deep hole is shown in Fig. 12a. An aspect ratio of 25 was obtained with deep holes for producing very straight walls. However, many cracks and chips with sizes over $30\ \mu\text{m}$ were produced. The average abrasive grain size of the diamond tool was $15\text{--}37\ \mu\text{m}$. The chipping decreased when the rotational speed was increased to 8000 rpm, as shown in Fig. 12b. Similar results have been obtained for machining a 5-mm-thick Pyrex 7740 substrate (Kalek et al. 2007).

The experiment results were measured by microscope and captured the picture to calculate the chipping area. The measure values include hole diameter r , maximum chipping diameter R . Then the average chipping length L can be calculated, and it could be expressed as follow:

$$L = R - r = ((A - a)/\pi)^{1/2} \tag{1}$$

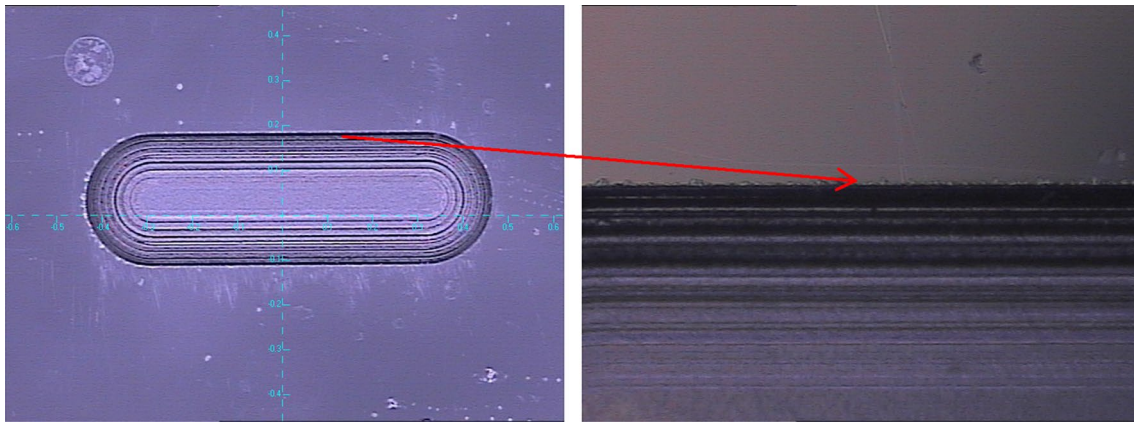


Fig. 11 Top-view optical micrograph of high slenderness ratio (width/depth) microfluidic channel in quartz

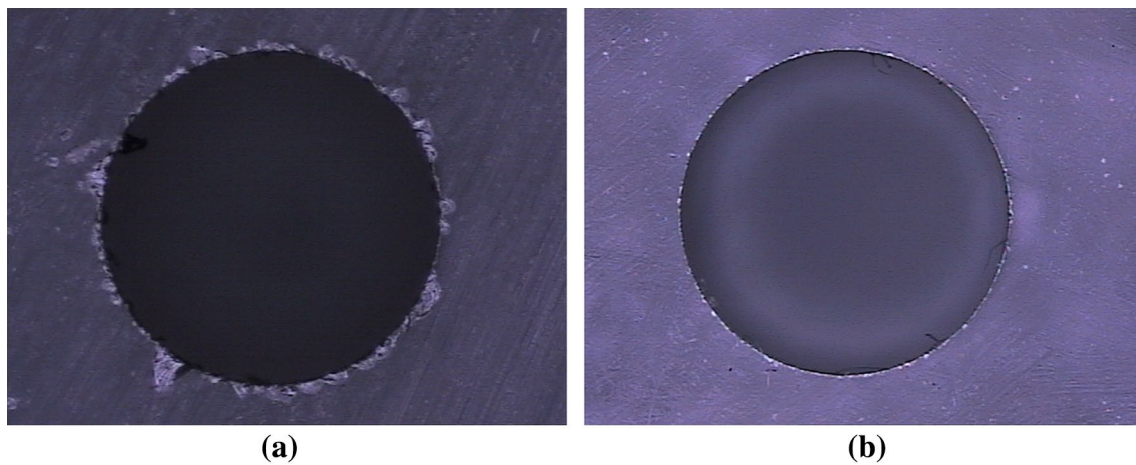


Fig. 12 Through-hole (1 mm in diameter) in 25-mm-thick quartz machined using with **a** rotational speed of 6000 rpm, feed rate of 8 mm/min, and 37- μ m abrasive grains and **b** rotational speed of 8000 rpm, feed rate of 8 mm/min, and 15- μ m abrasive grains

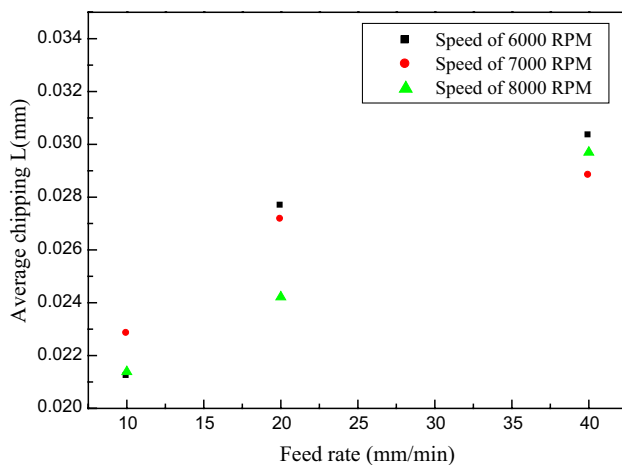


Fig. 13 Average chipping as a function of feed rate at speed of 6000, 7000, and 8000 rpm

where A is the maximum chipping area, a is hole area, R means the maximum chipping radius, and r stand for hole radius. Figure 13 shows the machining parameters of ultrasonic drilling. The machining parameters were: a rotational speed of 6000, 7000, and 8000 rpm, a feed rate of 10, 20, and 40 mm/min. When the feed rate was increased from 10 to 40 mm/min, the chipping was increased by around 30 %. However, it is very interesting to note that as the rotational speed was increased, the average chipping is about the same. Hence, for best surface quality, the feed rate should be low and the abrasive grain size of the diamond tool should be small.

4 Conclusion

This paper investigated the microfluidic channel fabrication process and compared picosecond laser machining, micro

ultrasonic machining, and ultra-precision machining for quartz material. Using picosecond laser and ultra-precision machining, the microstructure could be systematically controlled by adjusting the machining parameters. Picosecond laser machining with a short focal length could produce U- and \perp -shaped microfluidic channels. However, the surface roughness and surface quality were poor. The inner wall of the microfluidic channel has a relatively high surface roughness and a lot of slag. To achieve high surface quality, the micro-channel surface roughness (R_a) was less than $0.27\ \mu\text{m}$ was obtained by using ultra-precision machining. The microfluidic channel surface was very smooth, without chipping and cracks.

In addition, a deep hole with an aspect ratio of 25 was machined into quartz using micro ultrasonic machining. Chipping can be decreased by increasing the rotational speed and size of abrasive grains.

Acknowledgments The support from the Ministry of Economic Affairs and Micro/Meso Mechanical Manufacturing R&D Department, Taiwan, through Grants A0245010 and A0245020 is gratefully acknowledged.

References

- Anderson DG, Xu QB, Hashimoto M, Whitesides GM, Langer R (2009) Preparation of monodisperse biodegradable polymer microparticles using a microfluidic flow-focusing device for controlled drug delivery. *Small* 5:1575–1581
- Bhuyan MK, Courvoisier F, Lacourt PA, Jacquot M, Furfaro L, Withford MJ, Dudley JM (2010) High aspect ratio taper-free micro-channel fabrication using femtosecond Bessel beams. *Opt Express* 18:566–574
- Bokenkamp D, Desai A, Yang X, Tai YC, Marzluff E, Mayo S (1998) Microfabricated silicon mixers for submillisecond quench-flow analysis. *Anal Chem* 70:232–236
- Borghi A, Gualtieri E, Marchetto D, Moretti L, Valeri S (2008) Tribological effects of surface texturing on nitriding steel for high-performance engine applications. *Wear* 265:1046–1051
- Brivio M, Verboom W, Reinhoudt DN (2006) Miniaturized continuous flow reaction vessels: influence on chemical reactions. *Lab Chip* 6:329–344
- Chu LY, Utada AS, Shah RK, Kim JW, Weitz DA (2007) Controllable monodisperse multiple emulsions. *Angew Chem Int Ed* 46:8970–8974
- Dittrich PS, Manz A (2006) Lab-on-a-chip: microfluidics in drug discovery. *Rev Drug Discov* 5:211–218
- Gattass RR, Mazur E (2008) Femtosecond laser micromachining in transparent materials. *Nat Photon* 2:219–225
- Hettiarachchi K, Talu E, Longo ML, Dayton PA, Lee AP (2007) On-chip generation of microbubbles as a practical technology for manufacturing contrast agents for ultrasonic imaging. *Lab Chip* 7:463–468
- Hisamoto H, Saito T, Tokeshi M, Hibara A, Kitamori T (2001) Fast and high conversion phase-transfer synthesis exploiting the liquid–liquid interface. *Chem Commun* 24:2662–2663
- Kalek C, Robert L, Boy JJ, Blind P (2007) Deep microstructuring in glass for microfluidic applications. *Microsyst Technol* 13:447–453
- Leng XF, Zhang WH, Wang CM, Cui L, Yang CY (2010) Agarose droplet microfluidics for highly parallel and efficient single molecule emulsion PCR. *Lab Chip* 10:2841–2843
- Liu C, Liao Y, He F, Shen Y, Chen D, Cheng Y, Xu Z, Sugioka K, Midorikawa K (2012) Fabrication of three-dimensional microfluidic channels inside glass using nanosecond laser direct writing. *Opt Express* 20:4291–4296
- Menezes PL, Kailas, Kishore SV, Lovell MR (2010) Response of materials during sliding on various surface textures. *J Mater Eng Perform* 20:1438–1449
- Mitchell MC, Spikmans V, de Mello AJ (2001) Microchip-based synthesis and analysis: control of multicomponent reaction products and intermediates. *Analyst* 126:24–27
- Nakano M, Korenaga A, Miyake K, Murakami T, Ando Y, Usami H, Sasaki S (2007) Applying micro-texture to cast iron surfaces to reduce the friction coefficient under lubricated conditions. *Tribol Lett* 28:131–137
- Queste S, Salut R, Clatot S, Rauch JY, Malek CGK (2010) Manufacture of microfluidic glass chips by deep plasma etching, femtosecond laser ablation, and anodic bonding. *Microsyst Technol* 16:1485–1493
- Stroock AD, Dertinger SKW, Ajdari A, Mezi' C, Stone I, Whitesides GM (2002) Chaotic mixer for microchannel. *Science* 295:647–651
- Utada AS, Lorenceau E, Link DR, Kaplan PD, Stone HA, Weitz DA (2005) Monodisperse double emulsions generated from a microcapillary device. *Science* 308:537–541
- Yang Z, Matsumoto S, Goto H, Matsumoto M, Maeda R (2001) Ultrasonic micromixer for microfluidic systems sensor. *Actuat A-Phys* 93:266–272
- Zhang J, Midorikawa K (1999) High-quality and high-efficiency machining of glass materials by laser-induced plasma-assisted ablation using conventional nanosecond UV, visible, and infrared lasers. *Appl Phys A* 69:S879–S882
- Zhang J, Sugioka K, Midorikawa K (1998) High-speed machining of glass materials by laser-induced plasma-assisted ablation using a 532-nm laser. *Appl Phys A* 67:499–501
- Zhang B, Tice JD, Ismagilov RF (2004) Formation of droplets of in microfluidic channels alternating composition and applications to indexing of concentrations in droplet-based. *Anal Chem* 76:4977–49782
- Zhang H, Tumarkin E, Peerani R, Nie Z, Sullan RM, Walker GC, Kumacheva E (2006) Microfluidic production of biopolymer microcapsules with controlled morphology. *J Am Chem Soc* 128:12205–12210
- Zheng HY, Lee T (2005) Studies of CO₂ laser peeling of glass substrates. *J Micromech Microeng* 15:2093–2097